Experimental analysis of charging and discharging processes, with parallel and counter flow arrangements, in a molten salts high temperature pilot plant scale setup

Gerard Peiró[1], Jaume Gasia[1], Laia Miró[1], Cristina Prieto[2], Luisa F. Cabeza[1,*]

[1]GREA InnovacióConcurrent, Universitat de Lleida, Edifici CREA, Pere de Cabrera s/n, 25001, Lleida, Spain

[2]Abengoa Research. C/Energía Solar 1,41012, Seville, Spain

*Corresponding author: Tel: +34.973.00.35.76. Email: lcabeza@diei.udl.cat

Abstract

Despite the fact that there are some commercial concentrated solar power plants worldwide, there is currently a lack of experimental reports about the operational characteristics of this type of plants. Therefore, a two-tank molten salts thermal energy storage (TES) pilot plant at the University of Lleida (Spain) was used to analyse charging and discharging processes under real conditions. In this facility, 1000 kg of molten salts are used as TES material and Therminol VP-1 is used as heat transfer fluid (HTF). This facility is equipped with measurement equipment which allows an exhaustive analysis of the processes. In this study, the fact of varying the flow arrangement in the heat exchanger (parallel and counter flow arrangements) and the temperature difference between the molten salts and the HTF have been studied and discussed in terms of temperature profiles, energy and power stored/released from/to both HTF and molten salts, efficiencies and effectiveness. The best working conditions found were counter flow arrangement with a temperature grading of about 65 ºC.

Keywords: Concentrated solar power; sensible heat storage; two-tank; molten salts; heat exchanger; parallel flow arrangement; counter flow arrangement.

Nomenclature

C	Heat capacity, J/K
cp	Specific heat, J/kg·K
E	Energy, J
$\dot{m}$	Mass flow rate, kg/s
Q	Power, W

Greek symbols

ΔT	Temperature difference, ºC
Δt	Process length, s
ε	Effectiveness of the heat exchange, -
η	Efficiency of the heat exchange, -

Subscripts

act	Actual
HTF	Heat transfer fluid
in	Inlet
max	Maximum
min	Minimum
out	Outlet
salts	Molten salts

1 Introduction

Since 2010, generation of solar thermal electricity from concentrating solar power (CSP) plants has strongly grown worldwide. These plants generate electricity from renewable energy sources while producing no greenhouse gas (GHG) emissions, so it is considered to be a key technology to mitigate climate change and to achieve the reduction goals of GHG. In addition, the flexibility of CSP plants enhances energy security. Tomislav et al. [1] reviewed the existing CSP plants worldwide in order to identify their technical characteristics and operation conditions, and to extend their construction and use. Moreover, Reddy et al. [2] presented a state of the art of solar thermal power plants. They technically and economically compared three CSP plants case studies with different solar collection technologies in Indian tropical climates: parabolic through collector, parabolic dish collector and solar power tower. They concluded that parabolic dish with Stirling engine generates electricity at lower cost than the other technologies because of its higher efficiency, but has a lower yearly power output. In both studies [1,2], the parabolic through collector technology is highlighted as the most developed and mature technology in current commercially operating plants.

According to the International Energy Agency [3], when combined with thermal storage capacity of several hours of full-capacity generation, CSP plants can continue producing electricity when power demand steps up even when clouds block the sun, after sundown or in early morning. This effect is known as peak shaving (Figure 1). Zhang et al. [4] studied how thermal energy storage (TES) improved the competitiveness of the CSP technology in comparison with different fossil fuel fired backup systems. Those authors highlighted that accurate estimation of the direct daily solar irradiation is needed in order to design CSP and size TES or backup system, and concluded that in the future the solar energy contribution will increase due to technical improvement in solar collection and, in consequence, the required backup will be smaller.

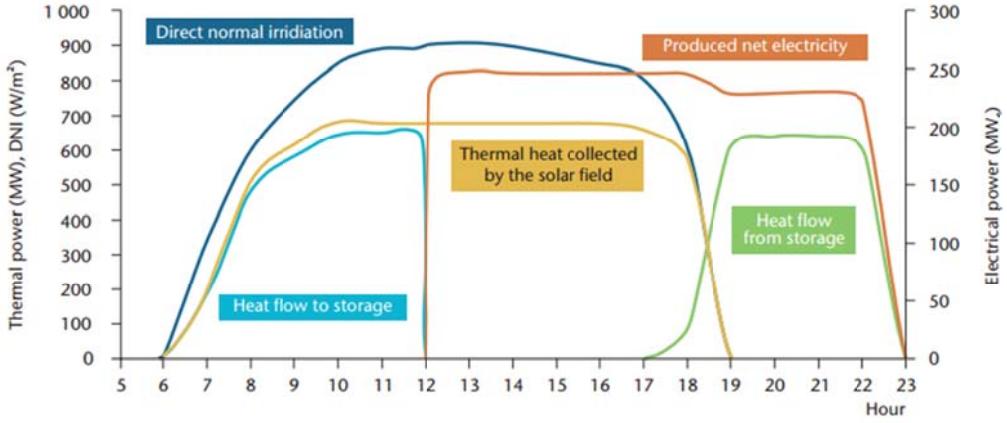

Figure 1. Peak shaving due to the use of thermal energy storage [3].

Already in 2010, Medrano et al. [5] reviewed the experiences in TES for power generation, showing the case studies available in the early stage pilot plants (such as Solar One and Solar Two) to commercial cases (such as PS10). Recently, Liu et al. [6] reviewed the current CSP plants and their TES systems and found that, up to March 2015, the CSP market had a total capacity of 5840 MWe worldwide, among which 4800 MWe is operational and 1040MWe is under construction. Spain had a total operational capacity of 2405 MW and 100 MW were under construction, turning out to be the world's leading country in CSP. Slightly less than half of the installed CSP capacity is integrated with thermal storage. However, taking a look to the facilities which are under construction, it is observed that over 80% of their capacity has energy storage.

Currently, the most developed and used TES system in commercial CSP plants is the indirect two-tank molten salt. This system uses as TES material the eutectic mixture of 60% of $NaNO_3$ and 40% of KNO_3, usually known as molten salts or solar salt, which are stored in two different storage tanks depending on their temperature level. Temperatures usually go from 292 ºC at the cold tank to 385 ºC at the hot tank. These operational temperatures are due to the salts melting temperature range and to the HTFs thermal stability limit (about 400ºC). TES processes in indirect two-tank molten salt are divided in three steps: charging, storage and discharging. During the charging process, the energy is collected by the HTF at the solar field (nominal temperatures of 391-393 ºC), and transferred to the molten salts in the HTF-molten salts heat exchanger. Molten salts are pumped from the cold tank at 292 ºC through the heat exchanger, arriving to the hot tank at a maximum storage temperature of 385ºC, where they are stored. When the energy stored is needed, the discharging process takes place, and the system operates in reverse form.

The behaviour of all main components of the two-tank storage system, such storage tanks, have been widely simulated [7] and tested at different scales pilot plant [8, 9] and at commercial scale [10] but not the heat exchanger. Hermann et al. [11] stated that heat exchanger should be designed within a small approach (3-10ºC) to maintain HTF supply temperature to the collector field during the charging process and minimize the performance penalty in the power block during the discharging process. Moreover, the heat exchanger should correctly operate under differential pressures between the HTF and molten salts side. Hence, it is crucial to understand the heat transfer process in HTF-molten salts heat exchanger in order to improve the performance and efficiency of the TES system and CSP plants.

Heat transfer processes in heat exchangers have been widely studied in the literature. Kakaç and Liu [12] showed the most common methods for the design, selection and sizing of different types of heat exchangers for different applications. The most widely used heat exchanger in commercial CSP plants is the shell-and-tube heat exchanger because of economic aspects [13]. Experimental and numerical work found in literature studied different features of performance of molten salts and HTF in shell-and-tube heat exchangers [14]. However, current CSP plants are starting to use plate heat exchangers because of their high thermal efficiency, compactness and flexibility against changes in load operation [15]. Walraven et al. [16] realised a comparison of shell and tube with plate heat exchangers in organic Rankine cycle for low temperature power generation applications and established that plate heat exchangers have a better performance under the same conditions but one disadvantage of plate heat exchangers is that the geometry of both sides is the same. Therefore, there is no available literature studying the performance of a plate heat exchanger under real CSP conditions. Hence, the objective of this article is to fill such knowledge gap since it represents the first experimental work in the literature regarding this topic. Its originality lies in the fact that the present work studies the reliability of a plate heat exchanger with thermal oil and molten salts as working fluids under real operation conditions in two-tank molten salts TES system.

In the facility used to perform this study, 1000 kg of molten salts are used as TES material and Therminol VP-1 is used as heat transfer fluid. Moreover, this facility is equipped with measurement equipment which allows an exhaustive analysis of the processes. The effects of varying the flow arrangement in the heat exchanger and the inlet temperature difference between the salts and the HTF during the charging and discharging processes have been studied and discussed based on: temperature profiles, energy and power stored/released from/to the HTF and molten salts, efficiencies and effectiveness. These variations aimed to simulate real working conditions at commercial CSP plants.

2 Materials and methodology

2.1 Materials

Synthetic thermal oil Therminol VP-1 was used as HTF in the present experimentation because of its thermal stability at high temperatures. Therminol VP-1 is a clear, water white sediment free liquid HTF which consists of a eutectic mixture of 73.5% diphenyl oxide ($C_{12}H_{10}O$) and 26.5% diphenyl ($C_{12}H_{10}$). Table 1 shows the main thermophysical properties of Therminol VP-1.

Table 1.Thermophysical properties of Therminol VP-1 [17].

Properties	**Units**	**Values**
Thermal stability	[ºC]	430
Boiling point	[ºC]	257
Crystallization point	[ºC]	12
Flash point	[ºC]	110 - 124
Autoignition temperature	[ºC]	621
Density	[kg/m^3]	$\rho = -2.835 \cdot 10^{-6} \cdot T^3(^oC) + 1.235 \cdot 10^{-3} \cdot T^2(^oC) + 1.037 \cdot T(^oC) + 1094$
Specific heat	[kJ/kg·K]	$cp = 4.908 \cdot 10^{-11} \cdot T^4(^oC) - 3.960 \cdot 10^{-8} \cdot T^3(^oC) + 1.107 \cdot 10^{-5} \cdot T^2(^oC) + 1.439 \cdot 10^{-3} \cdot T(^oC) + 1.556$
Thermal conductivity	[W/m·K]	$\lambda = -1.687 \cdot 10^{-7} \cdot T^2(^oC) - 8.885 \cdot 10^{-5} \cdot T(^oC) + 0.138$
Kinematic viscosity	[m^2/s]	$\upsilon = -9.565 \cdot 10^{-19} \cdot T^5(^oC) + 1.417 \cdot 10^{-15} \cdot T^4(^oC) - 8.435 \cdot 10^{-13} \cdot T^3(^oC) + 2.574 \cdot 10^{-10} \cdot T^2(^oC) - 4.197 \cdot 10^{-8} \cdot T(^oC) + 3.318 \cdot 10^{-6}$
Vapor pressure	[kPa]	$P_v = 7.394 \cdot 10^{-5} \cdot T^3(^oC) - 3.527 \cdot 10^{-2} \cdot T^2(^oC) + 5.744 \cdot T(^oC) + 3.064 \cdot 10^2$

On the other hand, a eutectic mixture consisting of a 60 % of sodium nitrate ($NaNO_3$) and a 40 % of potassium nitrate (kNO_3), widely known as solar salts, was the TES material used in this study. This salts mixture is the most studied and used TES material in commercial applications. The main properties of the solar salts obtained from laboratory analyses performed by Abengoa [18] are shown in Table 2.

Table 2. Properties of molten salts [18].

Properties	Units	Values
Composition	[-]	$NaNO_3$/ KNO_3 (60/40 wt%)
Appearance	[-]	White crystalline in solid and clear yellow in liquid
Melting point	[ºC]	238-241
Density	[kg/m^3]	$\rho = 0.636 \cdot T(^oC) + 2089.905$
Specific heat	[kJ/kg·K]	$cp = 1.723 \cdot 10^{-4} \cdot T(^oC) + 1.443$
Thermal conductivity	[W/m·K]	$\lambda = 1.9 \cdot 10^{-4} \cdot T(^oC) + 0.443$
Kinematic viscosity	[m^2/s]	$\upsilon = -6.557 \cdot 10^{-14} \cdot T^3(^oC) + 1.05 \cdot 10^{-10} \cdot T^2(^oC) - 5.706 \cdot 10^{-8} \cdot T(^oC) + 1.112 \cdot 10^{-5}$

2.2 Experimental setup

The high temperature pilot plant facility located at the University of Lleida (Spain), whose overview can be seen in Figure 2, was the experimental setup used to carry out the experimentation presented in this study. The goal of this experimental setup is to simulate the charging and discharging processes of a real two-tank molten salts TES system for CSP plants but at lower scale. Therefore the same elements and instrumentation than the ones used in a real scale plant are placed in this facility, which are gathered into the following main systems: (1) The heating system, which consists of a 24 kWe electrical heater that on the one hand heats up the HTF simulating the energy source during the charging process and on the other hand it pumps the HTF through the piping of the HTF loop. In a real CSP plant this function is accomplished in the solar field by the solar collectors or the solar tower. (2) The cooling system, which consists on a 20 kWth air-HTF heat exchanger that cools down the HTF simulating a power block during the discharging process. In a real CSP plant this function is accomplished by the steam generator, where the steam to drive the different turbines is produced. (3) The storage system consists of two 0.57 m^3 molten salts storage tanks (the so-called hot and cold tanks due to its thermal level) made of stainless steel 316L and with an identical shape than the storage tanks of commercial plants. 2.5 kW molten salt pumps located at the top of each tank are the responsible to move1000 kg of molten salts through the molten salts loop. (4) The heat exchange system consists of a multiple pass plate heat exchanger (HP 76-38H supplied by Alfanova) and its objective is to carry out the heat exchange between the molten salts and the HTF. Its main characteristics are listed in Table 3. (5) The electrical tracing system consists of different metallic wires installed along the piping of the molten salts loop, which provide heat by the Joule effect in order to maintain the molten salts piping at a desired temperature (above the molten salts melting point) and therefore avoid solidification problems. (6) Finally, the data acquisition system, which consists of all the temperature, pressure and flow rate sensors as well

as the different dataloggers and a personal computer, is the system which records at a time interval of 30 s the data from all the systems and materials to further be processed and analyzed. The pilot plant facility is insulated with rockwool and the bottom of storage tanks with foamglass and refractory cement to minimize the heat losses to the surroundings. Specific information about the design, construction, start-up and operation of this experimental pilot plant can be found in Peiró et al. [19].

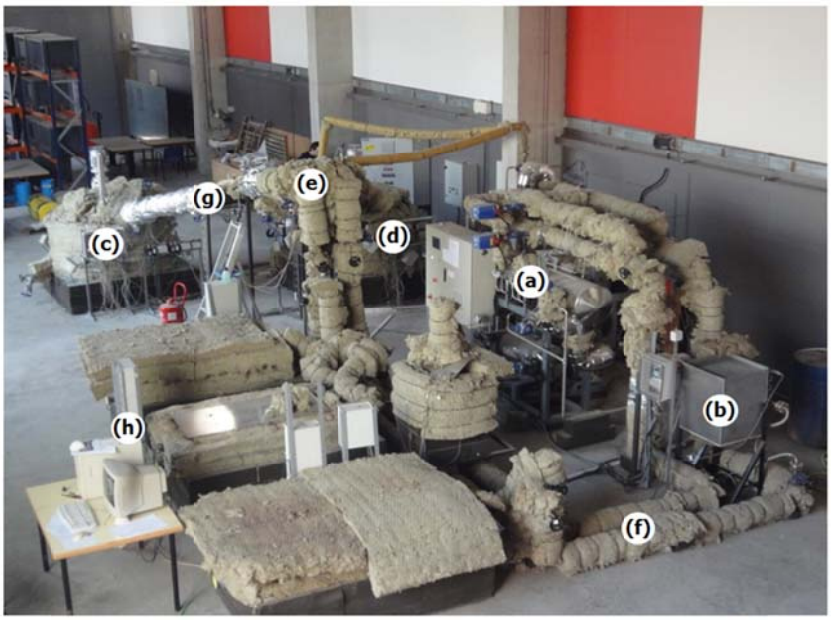

Figure 2. Overview of the pilot plant facility used to carry out the experimentation. (a) Electrical boiler, (b) Air-HTF heat exchanger, (c) Molten salts hot tank, (d) Molten salts cold tank, (e) HTF-molten salts heat exchanger, (f) HTF loop, (g) Molten salts loop and (h) Acquisition and recording system.

Table 3. Main characteristics of the heat exchanger used in the experimental set up.

Characteristics	**Thermal oil side**	**Molten salts side**
Design pressure	20 bar	10 bar
Test pressure	26 bar	13 bar
Design temperature	400 ºC	400 ºC
Directions of the fluids	Both	Both
Length x width x height	208 x 191 x 618 mm	
Plate material	Stainless steel alloy 316	
Plate thickness	0.40 mm	
Number of passes	10 (both sides)	
Number of plates	38	
Heat transfer area, A_{Exch}	3.8m^2	

In order to analyze the behavior of both the molten salts and the HTF during the charging and discharging processes, four temperature probes Pt-100with an accuracy of ± 0.1 ºC were installed in well insulated tube sections at 83 mm from the four terminals of the heat exchanger.

Moreover, the volumetric flow of the HTF was measured using a calibrated orifice plate with differential pressure transmitter, with an uncertainty of 0.2 %, located at the outlet of the electrical boiler. The molten salts volumetric flow is calculated using a homemade device which consists of a metallic tube that measures the molten salts level variation inside the tank during time intervals of five minutes.

2.3 Methodology

Four different operational modes are performed at the pilot plant facility depending on if it is a charging or a discharging process and on the flow arrangement of both the molten salts and the HTF: parallel or counter flow (Figure 3).

The charging process consists of storing the thermal energy in the molten salts by heating them up. In this process, the molten salts are pumped from the cold storage tank to the hot storage tank through the heat exchanger, where the energy from the HTF is transferred to the molten salts (Figure 3-a and Figure 3-c). The discharging process consists of releasing the thermal energy stored in the molten salts during the charging process by cooling them down. In this process, the molten salts are pumped from the hot storage tank to the cold storage tank through the heat exchanger, where the energy from the molten salts is transferred to the HTF (Figure 3-b and Figure 3-d).

In a parallel flow arrangement (Figure 3-a andFigure 3-b), the hot fluid and the cold fluid move in the same direction, while in a counter flow arrangement (Figure 3-c and Figure 3-d), the hot fluid and the cold fluid move in the opposite direction.

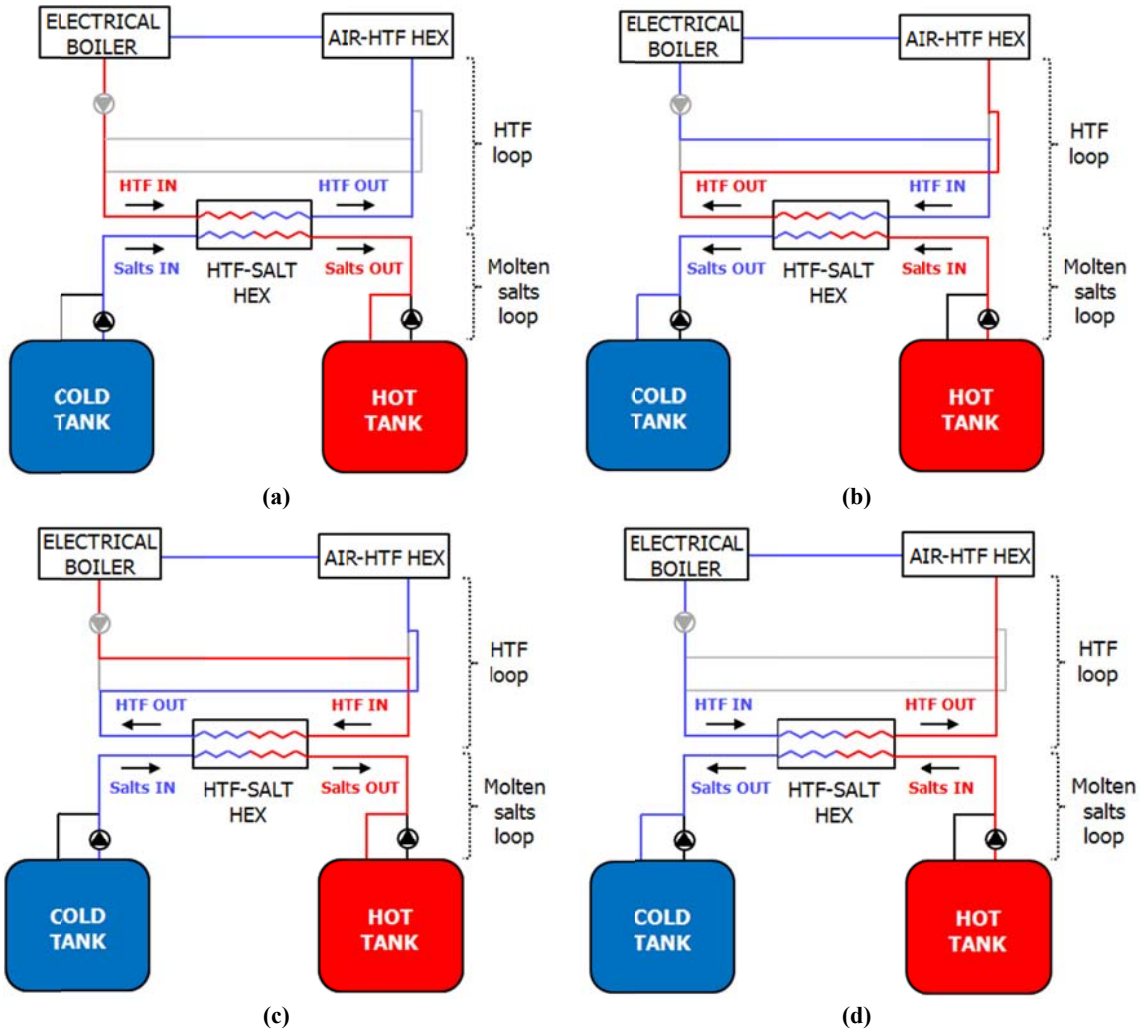

Figure 3.Operational modes of the pilot plant facility used to carry out the experimentation. (a) Charging process – parallel flow arrangement, (b) Discharging process – parallel flow arrangement, (c) Charging process – counter flow arrangement, (d) Discharging process – counter flow arrangement.

The experimentation carried out at the pilot plant facility and analyzed in the present study, consisted of six different experiments (Table 3) at constant mass flow rates of 0.09 kg/s and 0.11 kg/s for the HTF and molten salts, respectively. Charging and discharging processes with two different flow arrangements, parallel flow and counter flow, and two different inlet temperatures at the heat exchanger, 343±3 ºC and 373 ± 2 ºC, are shown and discussed.

Notice that HTF is flowing continuously, unlike molten salts which only flow during the charging and discharging processes in order to avoid possible plugs during the recirculation of the salts. In the previous and posterior preparation periods, "*Salts in* and *Salts out*" temperature sensors measure the temperature inside the piping, which is directly influenced by the electrical heat tracing.

Before starting each experiment, a recovery process of optimal temperature profiles according to the supplier was performed in order, on the one hand, to ensure a uniformity and homogeneity of the molten salts and the HTF at the initial temperatures and flow rates conditions and, on the other hand, to prepare the experimental setup for the desired flow rate arrangement. Once the initial conditions were set, the experiments started and were considered to be finished when the molten salts of the storage tank, from which the salts were pumped, reached the minimum operation level.

Table 4. Characteristics of the different experiments carried out at the pilot plant facility.

Experiment number	**Process**	**Flow arrangement**	**Temperature**	**ΔT**
#1	Charge	Parallel flow	*HTF in*: 343 ºC *Salts in*: 297 ºC	46 ± 3 ºC
#2	Discharge	Parallel flow	*HTF in*: 298 ºC *Salts in*: 341 ºC	
#3	Charge	Counter flow	*HTF in*: 341 ºC *Salts in*: 294 ºC	
#4	Discharge	Counter flow	*HTF in*: 297 ºC *Salts in*: 346 ºC	
#5	Charge	Counter flow	*HTF in*: 372 ºC *Salts in*: 303 ºC	68 ± 1 ºC
#6	Discharge	Counter flow	*HTF in*: 308 ºC *Salts in*: 375 ºC	

Notice that, regardless of the order in which the experiments are listed, each experiment is independent from the rest and their initial and final conditions have no connection between them.

2.4 Theory and calculation

In order to analyze and compare the charging and discharging processes described in the previous section, the following parameters have been taken into account: temperature evolution of the HTF and molten salts at the inlet and outlet of the heat exchanger, power and energy stored/released from/to the HTF and molten salts and the efficiency and effectiveness of the charging and the discharging processes.

The power released/absorbed by the molten salts and the HTF during the charging and discharging processes are described as Eq. (1) and Eq. (2) shows:

$$Q_{salts} = \dot{m}_{salts} \cdot cp_{salts} \cdot \Delta T_{salts_{in-out}} \quad (1)$$

$$Q_{HTF} = \dot{m}_{HTF} \cdot cp_{HTF} \cdot \Delta T_{HTF_{in-out}} \quad (2)$$

where $\dot{m}$ is the mass flow rate, cp is the specific heat obtained with the data shown at section 2.1, and ΔT is the temperature difference between the inlet and the outlet of the heat exchanger.

The energy obtained by the molten salts and by the HTF during the charging and discharging processes are described as Eq. (3) and Eq. (4) show:

$$E_{salts} = \dot{m}_{salts} \cdot cp_{salts} \cdot \Delta T_{salts_{in-out}} \cdot \Delta t \quad (3)$$

$$E_{HTF} = \dot{m}_{HTF} \cdot cp_{HTF} \cdot \Delta T_{HTF_{in-out}} \cdot \Delta t \quad (4)$$

where Δt is the process length.

The efficiency of the heat exchange during the charging and discharging processes is described as Eq. 5 and Eq. 6 show:

$$\eta_{charge} = \frac{Q_{salts}}{Q_{HTF}} \quad (5)$$

$$\eta_{discharge} = \frac{Q_{HTF}}{Q_{salts}} \quad (6)$$

And finally, the effectiveness of the heat exchange during the charging and discharging processes is defined by Eq. 7:

$$\varepsilon = \frac{Q_{act}}{Q_{max}} \quad (7)$$

where Q_{act} is the actual heat transfer and is calculated by Eq 8 and Q_{max} is the maximum possible heat exchanger rate with a given inlet temperatures and is defined by Eq. 9:

$$Q_{act} = \frac{Q_{HTF} + Q_{salts}}{2} \tag{8}$$

$$Q_{max} = C_{min} \cdot (T_{HTF_{in}} - T_{salts_{in}}) \tag{9}$$

where C_{min} is the lowest value between heat capacities of HTF and salts.

3 Results and discussion

3.1 Temperature profile

The temperature evolution along time and the average temperatures distribution of the HTF and molten salts at the cold tank side and hot tank side terminals of the heat exchanger for the six experiments above-explained are shown from Figure 4 to Figure 6. In these figures, the HTF temperature is represented in dotted lines while the molten salts are represented in straight lines. Moreover, in the charging process, the hot fluid is plotted in red and corresponded to the HTF while the cold fluid is plotted in blue and corresponded to the molten salts. In the discharging process, the hot fluid corresponded to the molten salts and the cold fluid corresponded to the HTF.

Before starting each charging process, there is no fluid circulation through the heat exchanger and therefore the piping, high values of temperature can be observed in both terminals because of the influence of the electrical tracing system on the temperature sensors. Similarly, before starting the each discharging process, inconsistent values of temperatures are observed because of the process preparation. From the HTF point of view, the decrease of temperatures corresponded to a fluid recirculation through the heat exchanger at the inlet HTF temperature while the variations of temperature on the molten salts side, were caused by the electrical tracing system. These periods are represented shaded in the all the figures which discuss the temperature profiles.

Regarding parallel flow arrangement, Figure 4 shows the temperature evolution along time and average temperature distribution at the two heat exchanger terminals during the experiments #1 and #2 (ΔT=46 ºC). At the beginning of the charging process (Experiment #1, Figure 4a and Figure 4c)a temperature difference of around 40 ºC could be observed at the cold tank side terminal of the heat exchanger (represented by the temperature sensors *HTF in* and *Salts in*). This temperature difference was increased 6 ºC as the process continued due to a decrease of the molten salts inlet temperature. The reason for such decrease lies on the fact that the temperature

of the molten salts stored on the cold tank was 297 ºC and therefore the electrical heating system was not that influent. On the other hand, at the hot tank side terminal of the heat exchanger (represented by the *HTF out* and the *Salts out*), the temperature difference was almost non-existent during the whole process, with a slightly decreasing tendency on their values because of the heat losses. At the beginning of the discharging process (experiment #2, Figure 4b), a temperature difference in the hot tank side terminal (represented by the temperature sensors *HTF in* and *Salts in*) of 32 ºC could be observed. This temperature difference was increased 12 ºC before achieving the steady state period as a result of the temperature at the hot storage tank (347 ºC) and the influence of the tracing system. At the cold tank side terminal (represented by the temperature sensors *HTF out* and *Salts out*) of the heat exchanger, the temperature difference decreased from around 10 ºC at the beginning of the process until 2 ºC in steady state.

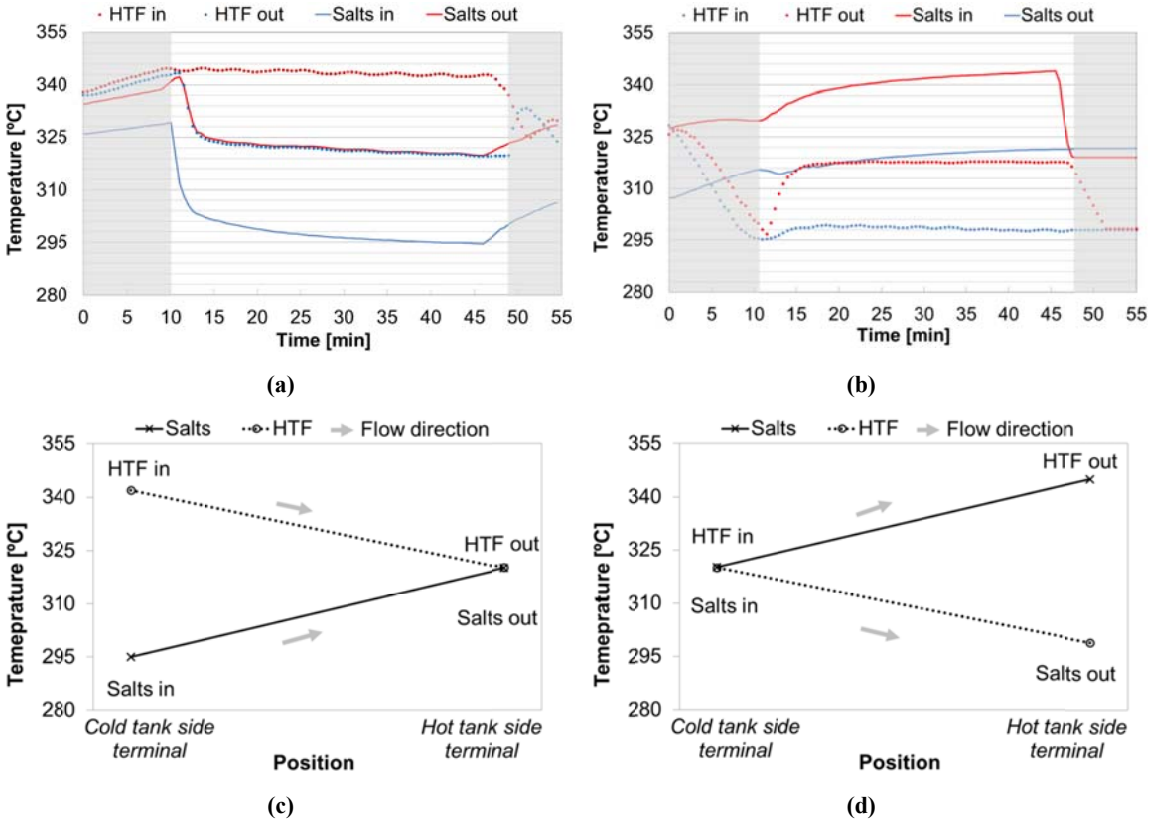

Figure 4. Temperature evolution along time and average temperature distribution of the HTF and molten salts at the four terminals of the heat exchange in a parallel flow arrangement: Experiment #1 – Charging process [(a) and (c), respectively] and during Experiment #2 – Discharging process [(b) and (d), respectively].

Regarding the counter flow arrangement, Figure 5 shows the temperature evolution along time and average temperature distribution at the two heat exchanger terminals during the experiments #3 and #4 (ΔT=46 ºC) and Figure 5 during the experiments #5 and #6 (ΔT=68 ºC). At the

beginning of the charging process (Experiment #3, Figure 5a and Figure 5c), no temperature difference could be observed at the hot tank side terminals of the heat exchanger (represented by the temperature sensors *HTF in* and *Salts out*) and as the process continued, the difference increased 5 ºC because of the achievement of the steady-state conditions. At the cold tank side terminals of the heat exchanger (represented by the temperature sensors *HTF out* and *Salts in*) the temperature difference was increased up to 5 ºC because of the decrease of the temperature of the inlet molten because of a lesser influence of the electrical tracing system. At the beginning of the discharging process (Experiment #4, Figure 5b and Figure 5d), the temperature difference at the cold tank side terminals (represented by the temperature sensors *HTF in* and *Salts out*)was 15 ºC and this value was decreased 10 ºC at the end of the process, while at the hot tankside terminals (represented by the temperature sensors *HTF out* and *Salts in*)the temperature difference was 5 ºC at the beginning of the process and 10 ºC at the end of the process. The reasons for this behavior are the same than in the previous case. The same behavior could be observed for experiments #5 and #6 in which the value of the HTF inlet temperature is higher and therefore the temperature gradient between the HTF and the molten salts was 68 ºC.

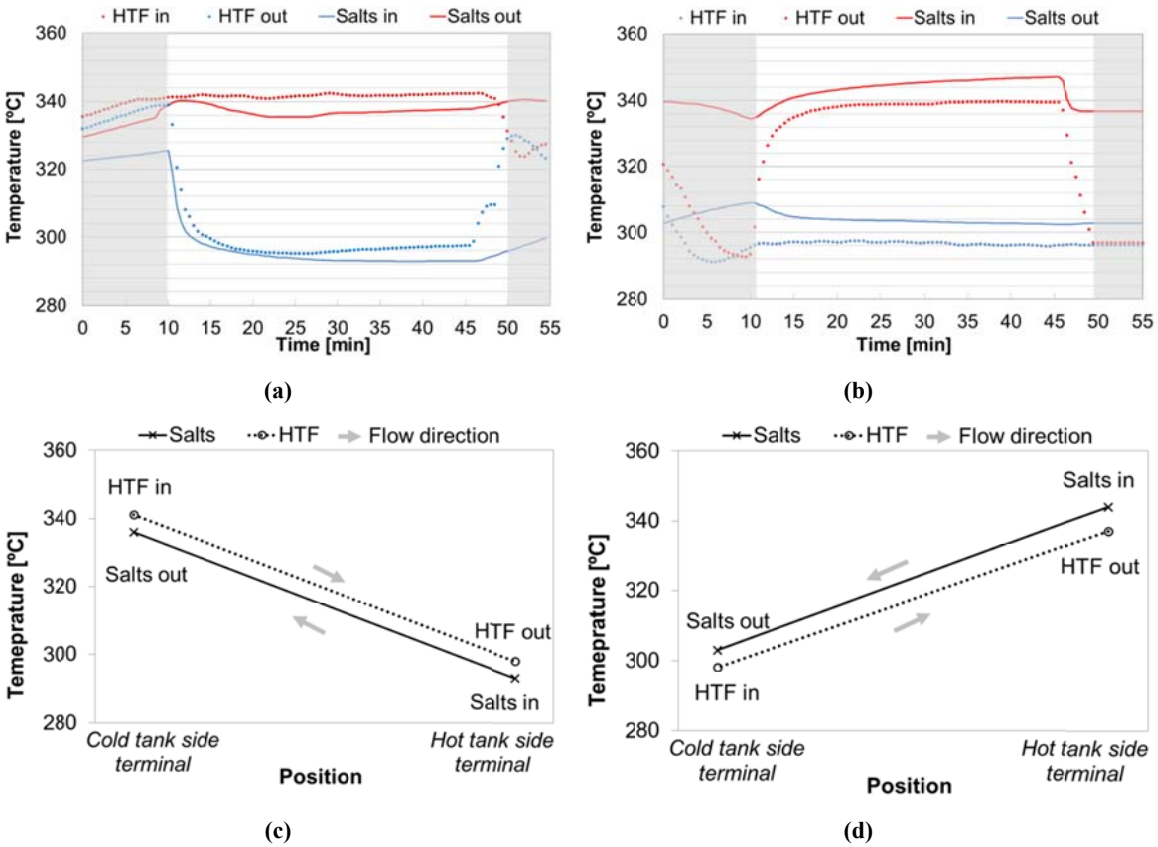

Figure 5. Temperature evolution along time and average temperature distribution of the HTF and molten salts at the four terminals of the heat exchange in a counter flow arrangement: Experiment #3 – Charging process [(a) and (c), respectively] and during Experiment #4 – Discharging process [(b) and (d), respectively].

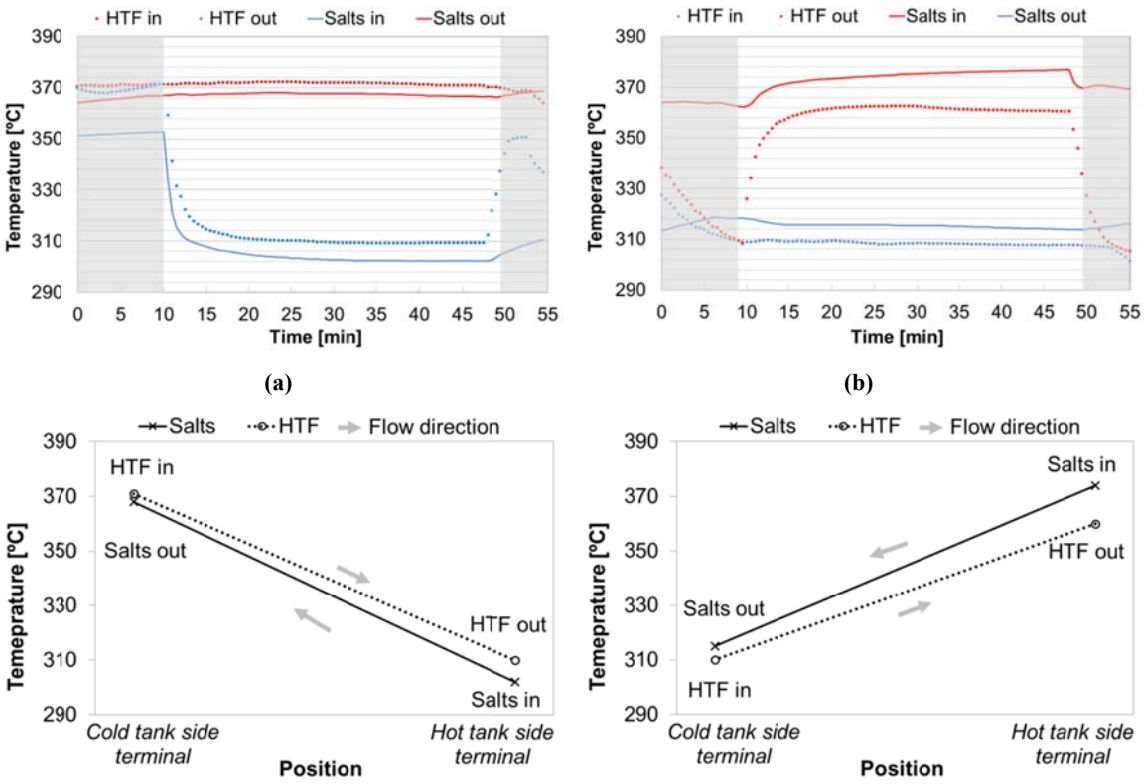

Figure 6. Temperature evolution along time and average temperature distribution of the HTF and molten salts at the four terminals of the heat exchange in a counter flow arrangement: Experiment #5 – Charging process [(a) and (c), respectively] and during Experiment #6 – Discharging process [(b) and (d), respectively].

Moreover, Figure 4c, 4d, 5c, 5d, 6c and 6d show the average temperature distribution of the HTF (discontinuous line) and molten salts (continuous line) at the cold tank and hot tank side terminals of the heat exchanger during the charging and discharging processes. The different heat exchanger arrangements can be identified: secant lines for the parallel flow (Figure4c and4d) and parallel lines for the counter flow arrangement (Figure5c, 5d, 6c, and 6d). If the counter flow arrangement (#3, #4, #5, #6) is compared to the parallel flow arrangement (#1 and #2), two main differences can be observed. First, the cold fluids (molten salts during charging and HTF during discharging) could achieve outlet temperatures 7 % higher in both processes. Second, the temperature difference between the molten salts and the HTF had a more uniformity and therefore a greater potential energy recovery.

3.2 Power and energy profiles

Figure 7 shows a comparison of the different power profiles of the HTF (represented in grey) and the molten salts (represented in black) during the charging (Figure 7a) and the discharging (Figure 7b) processes.

It can be observed that for the same inlet temperature gradient (comparing experiment #1 to #3 and experiment #2 to #4), the counter flow arrangement provides higher power values than the parallel flow arrangement (from 65.5to78.8 % higher) as a result of higher temperature gradients in the heat exchanger terminals and more constant thermal gradient between hot and cold fluid. Hence, these results extend the study cases where the benefits of the counter flow arrangement are experimentally shown.

For the same counter flow arrangement, it can be observed that the experiments with the highest temperature gradient (ΔT = 68 ºC) provide values of power 12.9 – 35.5 % higher in both processes of charging and discharging. The reason lies on the fact that incrementing temperature difference between the hot and cold fluid, increased the driving force for heat transfer and therefore entailed a higher power exchange.

When comparing charging and discharging processes in the same conditions, the combination of the heat losses and the non-ideal performance of the heat exchanger, cause the power from the HTF and the molten salts not being the same.

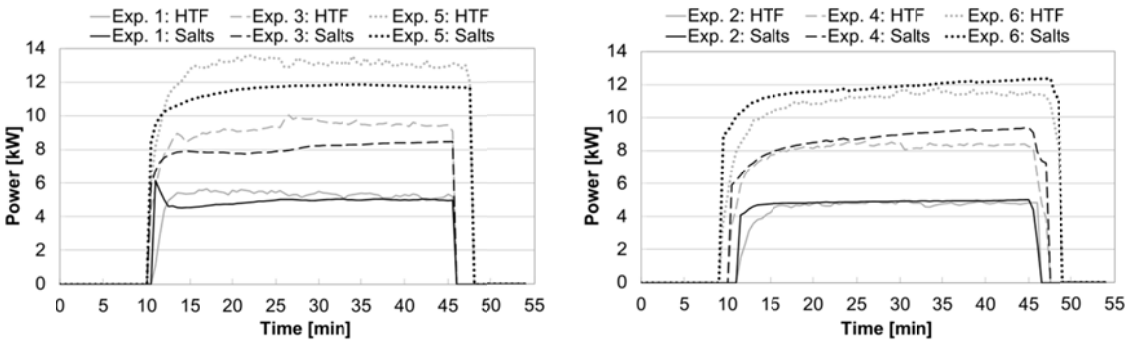

(a) **(b)**

Figure 7. Comparative of the different power profiles of the HTF (represented in grey) and the molten salts (represented in black) between the six different experiments performed during the (a) charging process and the (b) discharging process.

Regarding the energy, Figure 7 shows the comparative of the evolution in time of the amount of energy exchanged by the HTF and the molten salts in the six experiments performed. All of

them have a linear tendency, as expected, taking into account that during the steady process power has constant values. It can be observed that counter flow is more appropriate for maximum energy recovery. Energy reached at the end of the processes is shown in Table 4.

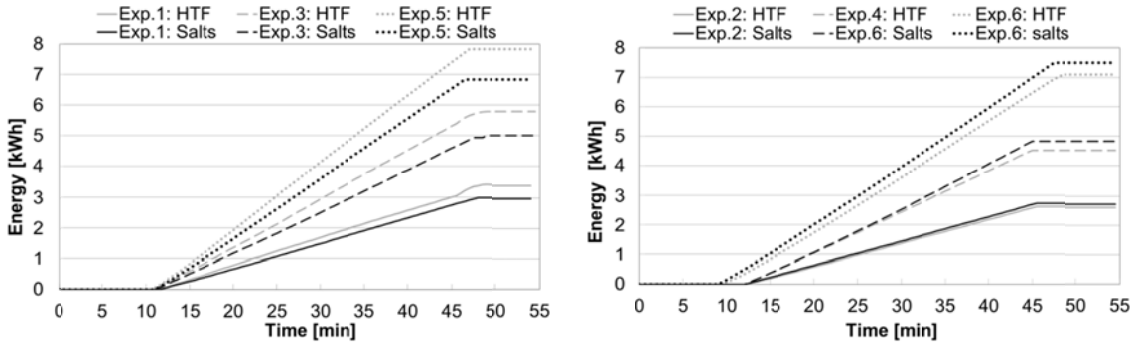

(a) **(b)**

Figure 8. Comparative of the different energy exchanged by the HTF (represented in grey) and the molten salts (represented in black), between the six different experiments performed during the (a) charging process and the (b) discharging process.

3.3 Efficiency and effectiveness profile

Figure 9 shows the evolution of experimental heat transfer effectiveness ratio during the charging (experiments #1, #3 and #5, Figure 9a) and discharging (experiments #2, #4 and #6, Figure 9b) processes. The values of effectiveness achieved in steady state conditions of all typologies of experiment are shown in Table 4.

As expected from the power exchanged results, the effectiveness ratio is higher in counter flow arrangement than parallel flow for the same initial conditions. In this case, the experiment #3 showed an enhancement of 66% in the effectiveness ratio in comparison with experiment #1. On the other hand, in the comparison of discharging processes (Experiment #2 and #4) an enhancement of 71% is observed.

For experiments in counter flow arrangement, the experiments the effectiveness ratio is almost the same regardless of the inlet temperature gradient. In this case the experiments #5 and #6 present only a 2-3% higher effectiveness ratio comparison with experiments #3 and #4.

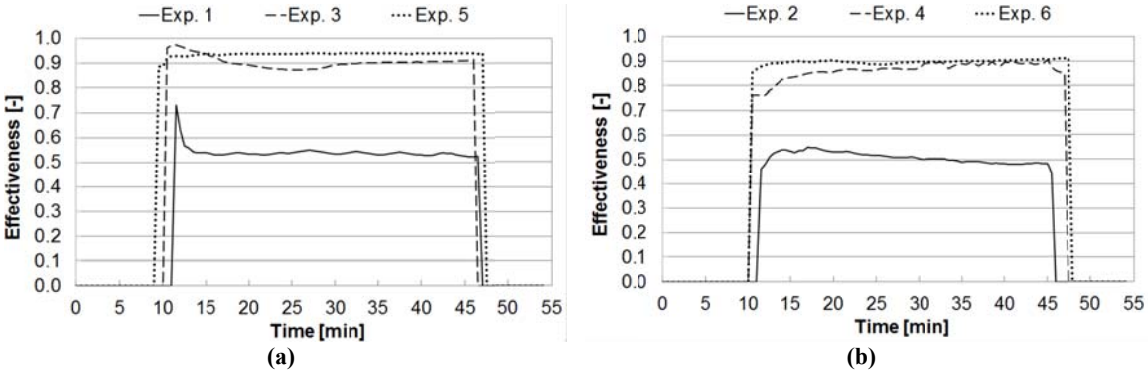

Figure 9. Experimental heat transfer effectiveness. (a) Charging and(b)Discharging processes.

In general the effectiveness ratio is 3-6%higher in all charging than discharging processes. But on the other hand the thermal performance is 4-6 % higher in discharging processes. This difference is due to higher thermal losses in the salts part of the heat exchanger and lower heat transfer in the salts.

4 Conclusions

Table 4 shows a summary of the most important results of the experiments carried out. The facility used in this study allows varying parameters like the heat exchanger flow arrangement (parallel and counter flow) and the inlet temperature difference at the terminals of the heat exchanger. Moreover, the facility is equipped with many measurement sensors which allow a detailed analysis of the performance. The parameters discussed during these processes are the molten salts and HTF temperature profiles, the energy and power stored/released from/to the HTF and molten salts, and the efficiencies and effectiveness of the charging and discharging processes. The main conclusion of all the study is that, as expected, in the same temperature conditions and temperature gradient, counter flow performs better than parallel flow; moreover, taking into account the same flow arrangement, the higher the inlet temperature, the better performance. The best working conditions are counter flow arrangement with a temperature gradient between 305 and 370 ºC.

Table 5.Summary of the most important results of the six experiments presented in this study.

Exp.	Process	Flow	ΔT [ºC]	Q_{HTF} [kW]	Q_{salts} [kW]	E_{HTF} [kWh]	E_{salts} [kWh]	η [-]	ε [-]
#1	Charge	Parallel flow	46 ± 3	5.34	4.90	3.40	2.97	0.92	0.54
#2	Discharge			4.72	4.85	2.61	2.72	0.97	0.57
#3	Charge	Counter flow		9.35	8.11	5.80	4.94	0.87	0.91
#4	Discharge			8.16	8.67	4.52	4.83	0.94	0.87
#5	Charge		68 ± 1	13.03	11.59	7.84	6.84	0.89	0.94
#6	Discharge			11.12	11.75	7.09	7.50	0.94	0.90

Acknowledgements

The research leading to these results has received funding from Spanish goverment (Fondo tecnológico IDI-20090393, ConSOLida CENIT 2008-1005) and from Abengoa Solar NT. The work is partially funded by the Spanish government (ENE2008-06687-C02-01/CON, ENE2011-28269-C03-02, ENE2011-22722 and ULLE10-4E-1305). The authors would like to thank the Catalan Government for the quality accreditation given to their research group GREA (2014 SGR 123). This project has also received funding from the European Commission Seventh Framework Programme (FP/2007-2013) under Grant agreement NºPIRSES-GA-2013-610692 (INNOSTORAGE) and from the European Union's Horizon 2020 research and innovation programme under grant agreement No 657466 (INPATH-TES). Laia Miró would like to thank the Spanish Government for her research fellowship (BES-2012-051861). Jaume Gasia would like to thank the Departament d'Universitats, Recerca i Societat de la Informació de la Generalitat de Catalunya for his research fellowship (2016FI_B 00047).The authors would like to thank Dr. Eduard Oró from Catalonia Institute for Energy Research (Spain) and Dr. Antoni Gil from Massachusetts Institute of Technology (USA) for their help during the initial stages of the experimentation.

References

[1] Pavlovic TM, Radonjic IS, Milosavljevic DD, Pantic LS. A review of concentrating solar power plants in the world and their potential use in Serbia. Renew Sust Energ Rev 2012; 16:3891-3902.

[2] Reddy SV, Kaushik SC, Ranjan KR, Tyagi, SK. State of the art of solar thermal power plants. A review. Renew Sust Energ Rev 2013;27:258–273.

[3] International Energy Agency. Technology Roadmap. Solar Thermal Electricity,

http://www.iea.org/publications/freepublications/publication/technologyroadmapsolarthermalelectricity_2014edition.pdf; 2014 [accessed 15.03.16].

[4] Zhang HL, Bayenes J, Degrève J, Cacères G. Concentrated solar power plants: Review and design methodology. Renew Sust Energy Rev 2013;22:466-481.

[5] Medrano M, Gil, A, Martorell I, Potau X, Cabeza LF. State of the art on high-temperature thermal energy storage for power generation. Part 2-Case studies. Renew Sust Energ Rev 2010;14:56-72

[6] Liu M, Tay NHS, Bell S, Belusko M, Jacob R, Will G, Saman W, Bruno F. Review on concentrating solar power plants and new developments in high temperature thermal energy storage technologies. Renew Sust Energ Rev 2016;53:1411-1432

[7] Zaversky F, García-Barberena J, Sánchez M, Astrain D. Transient molten salt two-tank thermal storage modelling for CSP performance simulations. Sol Energy 2013;93:294-311.

[8] Prieto C, Miró L, Peiró G, Oró E, Gil A, Cabeza LF. Temperature distribution in molten salts tank for CSP plant. Sol Energy. In press.

[9] Prieto C, Osuna R, Fernández AI, Cabeza LF. Molten salt facilities, lessons learnt at pilot plant scale to guarantee commercial plants; Heat losses evaluation and correction. Renew Energy 2016;94:175-185.

[10] Pacheco JE. Final test and evaluation results from the Solar two project. Sandia National Laboratories. 2002, [SAND2002-0120].

[11] Herrmann U, Kelly B, Price H. Two-tank molten salt storage for parabolic trough solar power plants. Energy 2004;29, 883-893.

[12] Kakaç S, Liu H. Heat exchangers: selection, rating, and thermal design. 1stt ed. Florida CRC Press LLC; 1998.

[13] Kelly B, Kearney D, Price H. Thermal storage commercial plant design study for a two-tank indirect molten salt system. National Renewable Energy Laboratory; 2006 [NREL/SR-550-40166].

[14] Zaversky F, Sánchez M, Astrain M. Object-oriented modelling for the transient response simulation of multi-pass shell-and-tube heat exchangers as applied in active indirect thermal energy storage systems for concentrated solar power. Energy 2014; 65: 647-664.

[15] Cristina Prieto (Abengoa), personal communication, April 27, 2016.

[16] Walraven D, Laenen B, D'Haeseleer W. Comparison of shell and tube with plate heat exchangers for the use in low-temperature organic Rankine cycles. Energ Convers Manage 2014;87:227-237.

[17] Therminol VP-1. Therminol VP-1 Heat transfer fluid product information, https://www.therminol.com/products/Therminol-VP1; [accessed 15.03.16]

[18] Peiró G, Gasia J, Miró L, Prieto C, Cabeza LF. Influence of the heat transfer fluid in a CSP plant molten salts charging process. Submitted to Renew Energy

[19] Peiró G, Prieto C, Gasia J, Miró L, Cabeza LF. Two-tank molten salts thermal energy storage system for solar power plants at pilot plant scale: lessons learnt and recommendations for its design, star-up and operation. Submitted to Sol Energy.